

Article

# High-Performance $\text{Na}_{0.44}\text{MnO}_2$ Slabs for Sodium-Ion Batteries Obtained through Urea-Based Solution Combustion Synthesis

Chiara Ferrara <sup>1</sup>, Cristina Tealdi <sup>1,\*</sup>, Valentina Dall'Asta <sup>1</sup>, Daniel Buchholz <sup>2,3</sup>,  
Luciana G. Chagas <sup>2,3</sup> , Eliana Quartarone <sup>1</sup>, Vittorio Berbenni <sup>1</sup> and Stefano Passerini <sup>2,3</sup> 

<sup>1</sup> Department of Chemistry and INSTM, University of Pavia, Via Taramelli 12, 27100 Pavia, Italy; chiara.ferrara01@universitadipavia.it (C.F.); vale.dallasta@gmail.com (V.D.); eliana.quartarone@unipv.it (E.Q.); vittorio.berbenni@unipv.it (V.B.)

<sup>2</sup> Helmholtz Institute Ulm (HIU), Helmholtzstraße 11, 89081 Ulm, Germany; daniel.buchholz@kit.edu (D.B.); luciana.chagas@kit.edu (L.G.C.); stefano.passerini@kit.edu (S.P.)

<sup>3</sup> Karlsruhe Institute of Technology (KIT), P.O. Box 3640, 76021 Karlsruhe, Germany

\* Correspondence: cristina.tealdi@unipv.it; Tel.: +39-382-98-7569

Received: 30 December 2017; Accepted: 31 January 2018; Published: 9 February 2018

**Abstract:** One of the primary targets of current research in the field of energy storage and conversion is the identification of easy, low-cost approaches for synthesizing cell active materials. Herein, we present a novel method for preparing nanometric slabs of  $\text{Na}_{0.44}\text{MnO}_2$ , making use of the eco-friendly urea within a solution synthesis approach. This kind of preparation greatly reduces the time of reaction, decreases the thermal treatment temperature, and allows the obtaining of particles with smaller dimensions compared with those obtained through conventional solid-state synthesis. Such a decrease in particle size guarantees improved electrochemical performance, particularly at high current densities, where kinetic limitations become relevant. Indeed, the materials produced via solution synthesis outperform those prepared via solid-state synthesis both at 2 C, (95 mA h g<sup>-1</sup> vs. 85 mA h g<sup>-1</sup>, respectively) and 5 C, (78 mA h g<sup>-1</sup> vs. 68.5 mA h g<sup>-1</sup>, respectively). Additionally, the former material is rather stable over 200 cycles, with a high capacity retention of 75.7%.

**Keywords:** sodium-ion battery; cathode; solution combustion synthesis; capacity retention;  $\text{Na}_{0.44}\text{MnO}_2$

## 1. Introduction

Energy storage is a key challenge of the present time. Academic and industrial research is focusing on the development of optimized materials and fabrication processes in order to meet stringent requirements in terms of electrochemical characteristics, while concomitantly achieving the preparation and commercialization of sustainable products, both from an economic and an environmental perspective [1]. For this reason, attention is being devoted to the search for and optimization of electrode compositions based on abundant and cheap chemical elements. In this context, research in the field of Na-ion battery materials is acquiring increasing importance, mainly due to the fact that, in line with the envisaged increasing demand of rechargeable batteries to implement electric vehicles, as well as portable and stationary applications, concerns have arisen with regard to the cost and availability of lithium in the near future [1,2]. The ability to replace or, better, to complement Li-ion technology with different metal ion chemistry, in particular Na-ions, would lower costs and alleviate such concerns [3,4]. In addition, the use of Na instead of Li metal allows the use of aluminum as an anode current collector, providing a cost-effective alternative to copper [2].

Mn-based compounds are being widely investigated as cathode materials for rechargeable Na-ion batteries and, in particular, sodium manganese oxides such as  $\text{Na}_{0.67}\text{MnO}_2$ ,  $\text{Na}_{0.44}\text{MnO}_2$  and other Na

compounds ( $\text{Na}_x\text{Mn}_y\text{B}_z\text{O}_2$ , B = transition metal) have been regarded as promising cathode materials due to their high capacity, low cost and non-toxicity [5,6]. Among various cathode materials for Na-ion batteries,  $\text{Na}_{0.44}\text{MnO}_2$  has been identified as highly promising because of its large capacity (theoretically  $121 \text{ mAh g}^{-1}$ ) and good stability [7], even in aqueous electrolyte [8,9].

$\text{Na}_{0.44}\text{MnO}_2$  (NMO) is characterized by a peculiar tunnel-like structure composed of Mn-based octahedra and square-based pyramids connected through a vertex to form small, distorted hexagonal channels and larger S-shaped tunnels running parallel to the  $c$  crystallographic axis (Figure 1). Three partially occupied Na sites are present within the structure. The Na-cations of all sites can be shuttled during the electrochemical redox process, but to different extents [10,11]. The high reversibility of the insertion and de-insertion processes is only guaranteed in the compositional range  $\text{Na}_{0.25}\text{MnO}_2$ – $\text{Na}_{0.65}\text{MnO}_2$ ; otherwise, the tunnel structure is not preserved [12].

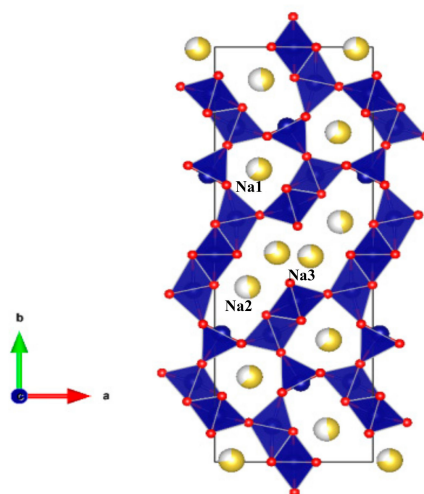


**Figure 1.** Crystal structure of  $\text{Na}_{0.44}\text{MnO}_2$  showing the partial site occupancy on the Na sites as partially colored spheres.

NMO powders are conventionally prepared by solid-state reaction at  $800 \text{ }^\circ\text{C}$  or higher for at least 9 h [10,13–15]. More recently, NMO materials have also been prepared by other synthesis procedures such as wet-chemistry techniques [12], including modified-Pechini methods [16–18], spray pyrolysis [19], polyvinylpyrrolidone (PVP)-assisted gel combustion synthesis [20,21], and reverse microemulsion methods [22,23]. However, even if a solution precursor is used, the NMO materials are usually obtained at high temperatures between  $800 \text{ }^\circ\text{C}$  [12,17,18] and  $950 \text{ }^\circ\text{C}$  [16,20,21] after several hours of annealing, typically ranging between 8 and 15 h. Notable exceptions are related to hydrothermal preparation strategies, where typically an aqueous solution is heated at only  $205 \text{ }^\circ\text{C}$ , but for 4 days, in an autoclave [24,25]. Quite surprisingly, NMO materials deliver similar electrochemical performance and specific capacities at low current rates (i.e., approaching the theoretical capacity of  $121 \text{ mA h g}^{-1}$ ), despite being synthesized via different methodologies.

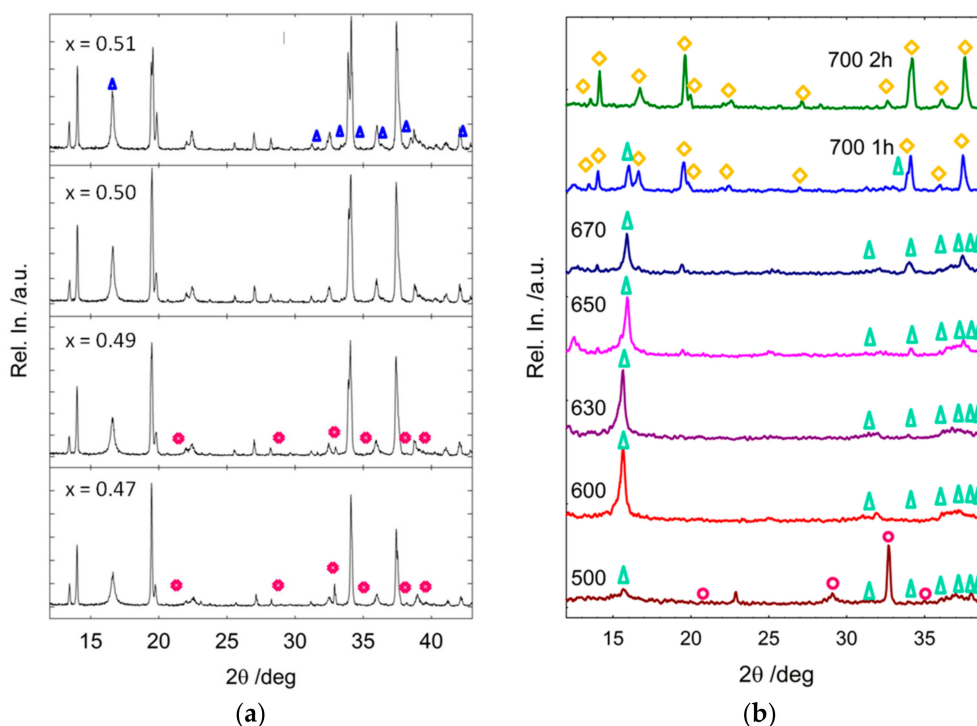
In this work, we explore the possibility of reducing the temperature and duration of the thermal treatment necessary to synthesize the environmental friendly NMO from abundant raw materials through a solution combustion approach. This synthetic approach involves a self-sustained reaction in an aqueous solution containing metal nitrates as oxidizers and urea as fuel and reducing agent [26,27]. Indeed, we demonstrate that such an energy-saving synthesis yields a material with high electrochemical performance, reduced energy cost, and lower environmental impact.

## 2. Results and Discussion

### 2.1. Structural and Morphological Characterization of the as Prepared SC-Powder

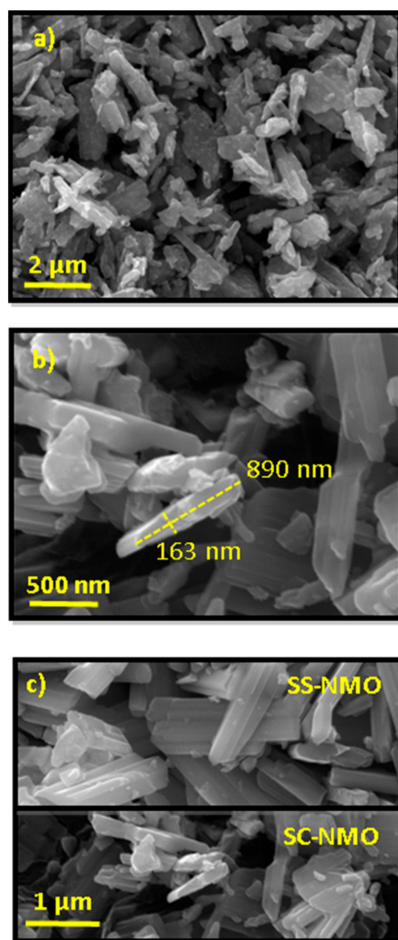
Prior to the electrochemical characterization, all materials underwent a structural investigation to identify the appropriate synthesis conditions. Figure 2a shows the X ray diffraction patterns, XRDP, of the samples prepared with different Na/Mn ratios in the range 0.47–0.51, treated at 800 °C for 2 h. Results show that the sample prepared with a nominal ratio of 0.50 is single-phase, with the desired structure of  $\text{Na}_{0.44}\text{MnO}_2$ , i.e., an orthorhombic *Pbam* space space group isostructural to  $\text{Na}_4\text{Mn}_4\text{Ti}_5\text{O}_{18}$  (JCPDS: 01-076-0785) [28]. Samples with a lower Na/Mn ratio (0.47 and 0.49) contain  $\text{Mn}_2\text{O}_3$  impurities (JCPDS: 01-71-0635), confirming a partial volatility of the alkali metal ions during the thermal treatment. Instead, the sample prepared with a higher Na content (Na/Mn ratio = 0.51) shows impurity peaks associated to the presence of  $\alpha\text{-NaMnO}_2$  (JCPDS: 01-25-0845).

Accordingly, the study on the required minimum temperature and time of the thermal treatment for obtaining single-phase  $\text{Na}_{0.44}\text{MnO}_2$  was performed with a Na/Mn ratio of 0.50. Figure 2b reports the evolution of the diffraction patterns at different annealing temperatures. The XRDP show that at least 700 °C is required to achieve the preparation of phase-pure  $\text{Na}_{0.44}\text{MnO}_2$  with the desired structure. Indeed, the mixture treated at 500 °C shows peaks related to the presence of crystalline  $\text{Mn}_2\text{O}_3$  (JCPDS: 01-71-0635), weak peaks due to  $\beta\text{-Na}_{0.70}\text{MnO}_2$  (JCPDS: 01-27-0752) and additional broader peaks of unidentified phases. After the thermal treatments at 600 °C, the dominant phase present is  $\beta\text{-Na}_{0.70}\text{MnO}_2$ , still partially detectable after the thermal treatment of 1 hour at 700 °C. Only after being treated at 700 °C for 2 h is the sample single-phase and able to be indexed according to the reflections of  $\text{Na}_{0.44}\text{MnO}_2$ , isostructural to  $\text{Na}_4\text{Mn}_4\text{Ti}_5\text{O}_{18}$  (JCPDS: 01-76-0193).



**Figure 2.** (a) X-Ray Diffraction Pattern, XRDP, of the samples prepared using different Na/Mn ratios in the precursor solution. Pink circles indicate the peaks of the  $\text{Mn}_2\text{O}_3$  impurity while blue triangles those of  $\alpha\text{-NaMnO}_2$ ; (b) XRDP of the  $\text{Na}_{0.44}\text{MnO}_2$  powders treated at increasing temperature. Pink circles indicate the peaks of the  $\text{Mn}_2\text{O}_3$  impurity, green triangles those of  $\beta\text{-Na}_{0.7}\text{MnO}_2$  and yellow squares are related to the  $\text{Na}_{0.44}\text{MnO}_2$  phase.

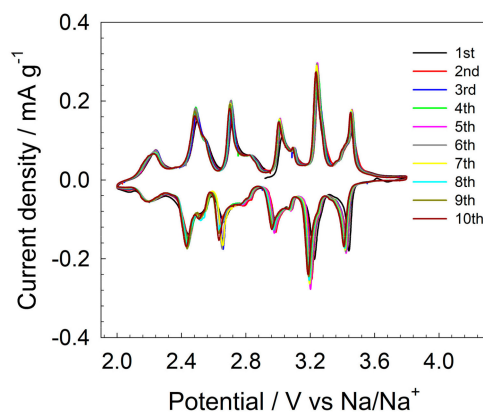
Figure 3 presents the SEM images of the sample prepared according to optimized solution combustion synthesis conditions (SC-NMO) and, as comparison, of the sample prepared according to the solid state route (SS-NMO). The scanning electron microscopy (SEM) images show that SC-NMO (Figure 3a,b) is mainly composed of sub-micrometric slabs of 100–400 nm width and 0.6–1.4  $\mu\text{m}$  length. Hence, the particle morphology of SC-NMO is similar to that of  $\text{Na}_{0.44}\text{MnO}_2$  reported in our previous work [29]. However, the dimensions of the SC-NMO slabs are smaller and surfaces of the slabs are less defined as compared to SS-NMO (Figure 3c). Heat treated  $\text{Na}_{0.44}\text{MnO}_2$  samples generally present rod-like structures due to the preferential growth along the [0 0 1] direction [22]. The present finding is therefore in agreement with the reduced time and temperature of the thermal treatment for SC-NMO compared to SS-NMO. Indeed, as expected, the synthetic approach here proposed is a solution-based approach. Wet-chemistry techniques are well known to produce even rather complex oxides at relative low temperatures, compared to conventional solid-state synthesis, thanks to the homogeneous and intimate mixing of the metal ions in the liquid phase and the formation of a porous matrix composed of nanoparticles that can easily react at the solid state in subsequent thermal treatments [30]. In addition, compared to other wet-chemistry techniques, the solution combustion approach takes advantage of the exothermicity of the redox reaction involved in the precursor formation; the released heat of the combustion reaction may fulfill, at least locally, the energy requirement for the formation of the oxide matrix, thus allowing the preparation of single-phase materials at relatively lower temperatures and in a shorter time [26].



**Figure 3.** Scanning Electron Microscopy, SEM, micrographs of the SC-NMO as synthesized powder. The magnifications are: (a) 25.0 kx and (b) 100.0 kx; (c) Comparison of two micrographs acquired at the same SEM mag. (50.0 kx): the upper image refers to SS-NMO sample; the lower one to SC-NMO sample.

## 2.2. Electrochemical Tests

Figure 4 shows the cyclic voltammetry (CV) scans of the SC-NMO electrode between 2.0 V–3.8 V. The general shape of the voltammograms, including the position of the current peaks, is in very good agreement with the literature. In detail, seven main anodic peaks (at 2.23, 2.49, 2.70, 3.00, 3.10, 3.23 and 3.45 V) and cathodic peaks (3.43, 3.22, 3.07, 2.97, 2.66, 2.43 and 2.19 V) are evident, confirming the reversibility of the process. Furthermore, each current peak is correlated to the (de)insertion of sodium from a particular crystallographic site [10,11]. Differently from what was observed with other morphologies, such as in NMO nanofibers [31], SC-NMO does not need an activation cycle: in fact, the current peaks of the first cyclic sweep are overlapping with those of the following cycles.



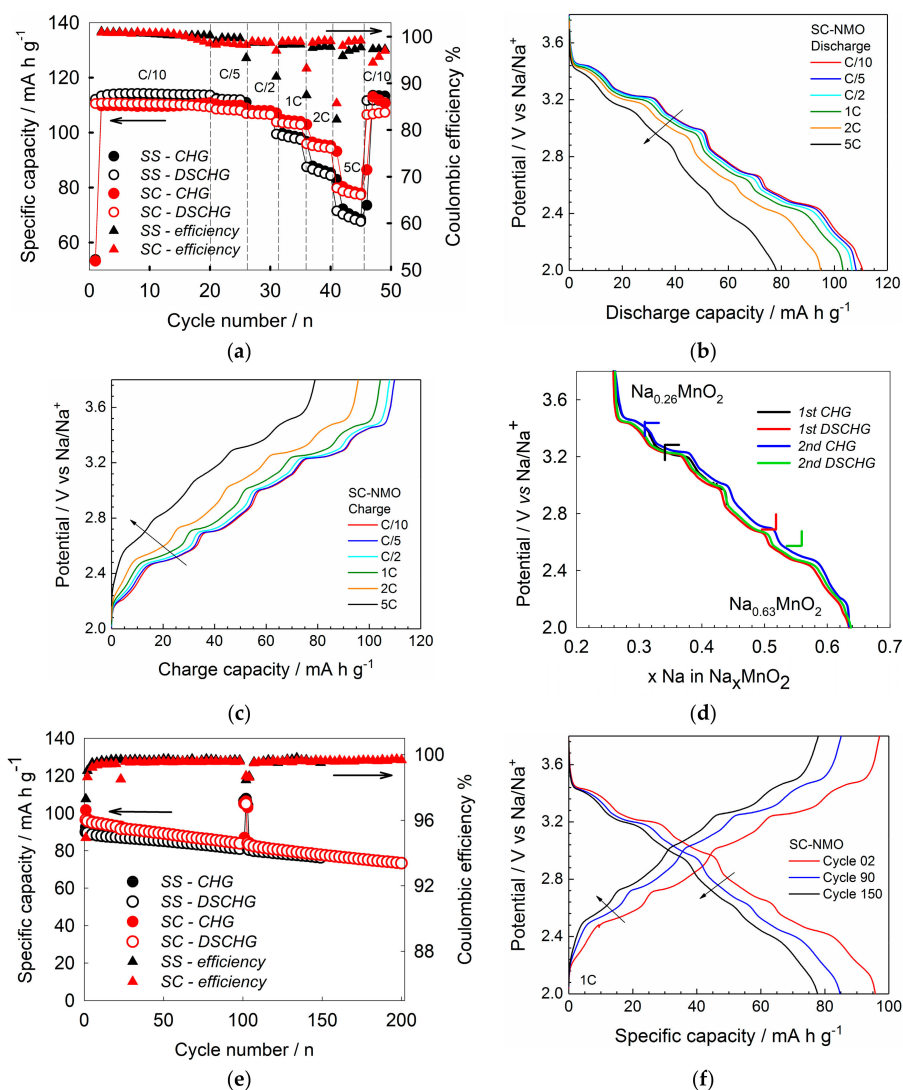
**Figure 4.** Cyclic Voltammetry, CV, of the SC-NMO tested for 10 cycles in the potential range 2.0 V–3.8 V with the electrolyte NaPF<sub>6</sub> 1M in PC.

Figure 5 reports the cycling performance of the SC-NMO at increasing C rates (C/10, C/5, C/2, 1 C, 2 C and 5 C) and during the long-term cycling test at 1 C. In addition, selected potential profiles of SC-NMO, recorded at different C-rates and during the 1st and 2nd cycle at C/10 are also given. The galvanostatic cycling data are compared with SS-NMO to reveal the impact of the modified synthesis conditions [29]. The capacities at C/10 are approximately 115 mA h g<sup>-1</sup>, i.e., in very good agreement with literature data and close to the theoretical capacity of 121 mA h g<sup>-1</sup>. For example, at the same C rate, a reversible capacity of 110 mA h g<sup>-1</sup> was reported for a sample prepared through solid state reaction at 800 °C for 9 h [14] and 112 mA h g<sup>-1</sup> for a sample prepared through a solution synthesis approach followed by a thermal treatment at 800 °C for 10 h [32].

At low current densities, such as C/10 or C/5, the SS-NMO-based electrode delivers only a slightly higher capacity of about 1–2 mAh g<sup>-1</sup>, both in charge and in discharge, which is within the margin of experimental error of the battery cycles used. However, at C/2, both materials show the same performance, and from 1 C on the SC-NMO outperforms SS-NMO in terms of delivered specific capacity and coulombic efficiency. At 1 C the difference is still small but at 2 C the capacity difference between the two materials increases to 10 mA h g<sup>-1</sup>, i.e., SC-NMO delivering 95 mA h g<sup>-1</sup> and SS-NMO only 85 mA h g<sup>-1</sup>. Both materials show a rather reversible behavior after the current rate test, i.e., when reducing the cycling rate at C/10.

It should be noted that the improved performance of SC-NMO at high C rates is not related to residual carbon coating, because the preparation of SC-NMO is performed in oxidizing atmosphere, i.e., air, to avoid the material's degradation. In fact, even in a slightly reducing atmosphere, such as nitrogen, the material degrades to a mixture of Mn<sub>2</sub>O<sub>3</sub> and Na<sub>2</sub>O, which readily transforms into NaCO<sub>3</sub> under ambient conditions (see Figure S1, Electronic Supplementary Information (ESI)). Consistently, the TGA traces (Figure S2, ESI) do not indicate for the presence of additional carbon. In fact, the degree of weight loss for the SS-NMO sample, prepared in the absence of organic reagents, is even higher than that pertaining to the SC-NMO sample during a first acquisition of the TGA curve.

The potential profiles during discharge and charge for the 3rd cycle at each C rate are reported in Figure 5b,c, respectively. The plateaus in the potential profiles correspond well with the current peaks observed via cyclic voltammetry in Figure 4. SC-NMO and SS-NMO were also cycled at 1 C for 200 cycles (Figure 5e) and selected potential profiles of SC-NMO upon cycling are shown in Figure 5f. After 100 cycles, 2 cycles at C/10 were performed to evaluate material degradation. As can be clearly seen in Figure 5e, the capacity of the SC-NMO material is always higher than the one of the SS. After 200 cycles the discharge capacity of SC-NMO is  $73.8 \text{ mA h g}^{-1}$  with a coulombic efficiency of 99.72% and a capacity retention of 75.7%. Interestingly, the SC-NMO capacity is completely retained (around  $108 \text{ mA h g}^{-1}$ ) when current is changed to C/10 after the long-term cycling at 1 C. This suggests that the fading performance during long-term cycling is correlated with the composite electrode degradation rather than the irreversible structural degradation of the active material.



**Figure 5.** (a) Comparison of the C rate tests performed on the SS-NMO-based electrode [29] and the SC-NMO-based electrode presented in this work: the tested C rates are: C/10, C/5, C/2, 1 C, 2 C, 5 C; (b,c) show the potential profiles of SC-NMO, respectively, during the 3rd discharge and charge cycle at each C rate; (d) “Potential vs.  $x \text{ Na}$  in  $\text{Na}_x\text{MnO}_2$ ” graph reported for the 1st and 2nd cycles at C/10. The arrows show if the material is increasing or decreasing its sodium content while cycling; (e) 1 C long-term cycling comparison between SC-NMO-based electrode (200 cycles) and SS-NMO-based electrode (150 cycles—reported in our previous work [29]); (f) selected potential profiles of SC-NMO upon cycling (panel e).

The high coulombic efficiency registered for the SC-NMO again suggests a highly reversible insertion of  $\text{Na}^+$  ions. Indeed, as reported in Figure 5d, the amount of  $\text{Na}^+$  equivalents in SC-NMO is between 0.63 eq.  $\text{Na}^+$  and 0.26 eq.  $\text{Na}^+$ , i.e., well within the range where high reversibility is observed [13]. As a matter of fact, the potential profiles of the first and second charge plotted vs.  $\text{Na}^+$  equivalents (Figure 5d) almost overlap.

### 3. Materials and Methods

#### 3.1. Solution Combustion Synthesis of $\text{Na}_{0.44}\text{MnO}_2$

The powder sample of nominal composition  $\text{Na}_{0.44}\text{MnO}_2$  (solution combustion synthesis  $\text{Na}_{0.44}\text{MnO}_2$ , SC-NMO) was prepared starting from appropriate amounts of  $\text{NaNO}_3$ ,  $\text{Mn}(\text{NO}_3)_2 \cdot 4\text{H}_2\text{O}$  and urea,  $\text{CO}(\text{NH}_2)_2$  (Sigma-Aldrich S.r.l, Milano, Italy). The chemicals were dissolved in deionized water in the appropriate stoichiometric ratio and heated at 80 °C under continuous stirring for 30 min. The temperature was then increased to 100 °C to achieve complete evaporation of the solvent until a viscous light pink resin was obtained, which spontaneously ignited to produce a black precursor. This latter was subsequently treated in a furnace at a temperature between 500 °C and 700 °C for maximum 2 h. The Na/Mn ratio was modified between 0.47–0.51 to identify the Na excess suitable to compensate for the loss of alkali metal during the high temperature synthesis steps.

For comparison, a sample of the same nominal composition (solid-state synthesis  $\text{Na}_{0.44}\text{MnO}_2$ , SS-NMO) was prepared according to the solid-state synthesis procedure reported by Sauvage et al. [13], which foresees a 10 wt.% excess of Na precursor, corresponding to a starting stoichiometry of  $\text{Na}_{0.49}\text{MnO}_2$ , to compensate for the Na ion volatility at high temperature. The characterization of this sample was already described in our previous work [29].

#### 3.2. Morphological and Structural Characterization of SC-NMO

SC-NMO powder was sputter-coated with Au and analyzed through Scanning Electron Microscopy (SEM, Mira 3, Tescan, Brno, Czech Republic), using a beam acceleration voltage of 20 kV. The average dimensions of the slabs were calculated by measuring the width and length of at least 75 single slabs through the ImageJ<sup>®</sup> free software. X-ray Diffraction Patterns (XRDP, BRUKER diffractometer D8 Advance, Cu-K $\alpha$ :  $\lambda = 0.154$  nm, Bruker Italia S.r.l., Milano, Italy) were acquired on the SC-NMO powder using an Al sample holder. The data were acquired in the  $2\theta$  range from 10° to 45° with scan step of 0.02 and a fixed counting time per step of 8 s. The powder underwent a Thermo-Gravimetric Analysis (TGA, Q5000, TA Instruments, New Castle, DE, USA) under static air, with a heating ramp of 10 °C/min from room temperature up to 800 °C.

#### 3.3. Casting of the Electrodes

The NMO (both SC or SS) powders were mechanically sieved (mesh size  $\leq 45$   $\mu\text{m}$ ), after hand-grinding to separate possible agglomerates of particles. The active material, the conductive carbon (SuperC65<sup>®</sup>, IMERYS, Switzerland) and binder polyvinylidene fluoride (PVdF, Solef 6020, Solvay Polymer specialties, Bruxelles, Belgium) were mixed via stirring overnight in N-methyl-2-pyrrolidone (NMP, Sigma Aldrich) in the weight ratio 85:10:5, respectively. In detail, 1 mL of NMP was used for 0.588 g of solid (solid content of 34.8%). Slurries with a wet thickness of 150  $\mu\text{m}$  were cast on aluminum foil (Hydro, 0.020 mm thick). The slurries were dried overnight in an oven at 60 °C, and then round disc electrodes with a diameter of 12 mm-diameter were cut. The electrodes were dried under vacuum in a glass oven (Büchi) for 3 h at room temperature, 3 h at 60 °C and finally for 12 h at 100 °C. Subsequently, electrodes were pressed (8 ton for 10 s), weighed and dried again under vacuum for 3 h at room temperature and 8 h at 100 °C. The final electrodes had an average active material mass loading of 2.7 to 3.2  $\text{mg cm}^{-2}$ .

### 3.4. Cell Assembly and Electrochemical Tests

Three-electrode Swagelok cells were assembled inside an argon-filled glove-box (mBraun) with water and oxygen content below 0.1 ppm. The cell configuration for all tests was: Na metal (99.8%, ACROS ORGANICS, Geel, Belgium) as reference and counter electrode (RE, CE), 1M NaPF<sub>6</sub> (sodium hexafluorophosphate, 99+%, FluoroChem, Glossop, UK) in PC (propylene carbonate, battery grade, BASF, Ludwigshafen, Germany) as electrolyte with glass fiber disks (GF/D, Whatman, Maidstone, UK) as separator and NMO as working electrode (WE). NaPF<sub>6</sub> and PC were used without further purification.

Electrodes (all possessing similar mass loading) were tested through cyclic voltammetry (CV) with a scan rate of 0.1 mV s<sup>-1</sup> in the potential range of 2.0 V–3.8 V vs. Na/Na<sup>+</sup> (VMP3 multichannel potentiostat, BioLogic, Seyssinet-Pariset, France). The galvanostatic cycling was performed between 2.0 V and 3.8 V at various current densities ranging from C/10 to 5 C (1 C = 121 mA g<sup>-1</sup>) (Maccor battery tester 4300, Maccor Inc., OK, USA). All electrochemical tests were carried out at 20 ± 1 °C.

## 4. Conclusions

For the first time, Na<sub>0.44</sub>MnO<sub>2</sub> nanometric slabs were synthesized using an urea-based solution combustion synthesis and a subsequent annealing process. This simple synthetic approach, which makes use of the eco-friendly urea, enabled the preparation of Na<sub>0.44</sub>MnO<sub>2</sub> cathode material in less time (2 h) and at a lower annealing temperature (700 °C) compared to state-of-the-art synthesis routes such as solid-state and sol-gel methods. SEM revealed smaller particle dimensions as a result of the aforementioned synthesis conditions. Moreover, the final cathode material has shown superior electrochemical performances, in terms of delivered capacities at high C rates of up to 5 C (i.e., 105 mAh g<sup>-1</sup> at 1 C and 80 mAh g<sup>-1</sup> at 5 C).

The improved capacities at high rates can be ascribed to the different morphology, i.e., smaller slabs characterized by a lower degree of anisotropy. Hence, the results suggest that reducing the particle sizes may be a suitable strategy for improving the high rate performances of Na<sub>0.44</sub>MnO<sub>2</sub> cathode materials.

**Supplementary Materials:** The following are available online at [www.mdpi.com/2313-0105/4/1/8/s1](http://www.mdpi.com/2313-0105/4/1/8/s1), Figure S1: XRDP of the NMO sample after a thermal treatment at 800 °C under N<sub>2</sub> flux, Figure S2: Thermogravimetric analysis of the SS- and SC-NMO powders.

**Acknowledgments:** L.G.C., S.P and D.B acknowledge the financial support of the Helmholtz Association. C.T. is grateful for the financial support of Fondazione Cariplo and Regione Lombardia through grant 2015-0753.

**Conflicts of Interest:** The authors declare no conflict of interest.

## References

1. Kundu, D.; Talaie, E.; Duffort, V.; Nazar, L.F. The Emerging Chemistry of Sodium Ion Batteries for Electrochemical Energy Storage. *Angew. Chem. Int. Ed.* **2015**, *54*, 3432–3448. [[CrossRef](#)] [[PubMed](#)]
2. Hwang, J.-Y.; Myung, S.-T.; Sun, Y.-K. Sodium-ion batteries: Present and future. *Chem. Soc. Rev.* **2017**, *46*, 3529–3614. [[PubMed](#)]
3. Kubota, K.; Komaba, S. Review—Practical Issues and Future Perspective for Na-Ion Batteries. *J. Electrochem. Soc.* **2015**, *162*, A2538–A2550. [[CrossRef](#)]
4. Yabuuchi, N.; Kubota, K.; Dahbi, M.; Komaba, S. Research Development on Sodium-Ion Batteries. *Chem. Rev.* **2014**, *114*, 11636–11682. [[CrossRef](#)] [[PubMed](#)]
5. Kim, H.; Kim, H.; Ding, Z.; Lee, M.H.; Lim, K.; Yoon, G.; Kang, K. Recent Progress in Electrode Materials for Sodium-Ion Batteries. *Adv. Energy Mater.* **2016**, *6*, 1600943.
6. Xiang, X.; Zhang, K.; Chen, J. Recent Advances and Prospects of Cathode Materials for Sodium-Ion Batteries. *Adv. Mater.* **2015**, *27*, 5343–5364. [[CrossRef](#)] [[PubMed](#)]

7. Cao, Y.; Xiao, L.; Wang, W.; Choi, D.; Nie, Z.; Yu, J.; Saraf, L.V.; Yang, Z.; Liu, J. Reversible Sodium Ion Insertion in Single Crystalline Manganese Oxide Nanowires with Long Cycle Life. *Adv. Mater.* **2011**, *23*, 3155–3160. [[CrossRef](#)] [[PubMed](#)]
8. Hung, T.F.; Lan, W.H.; Yeh, Y.W.; Chang, W.S.; Yang, C.C.; Lin, J.C. Hydrothermal Synthesis of Sodium Titanium Phosphate Nanoparticles as Efficient Anode Materials for Aqueous Sodium-Ion Batteries. *ACS Sustain. Chem. Eng.* **2016**, *4*, 7074–7079. [[CrossRef](#)]
9. Li, Z.; Young, D.; Xiang, K.; Carter, W.C.; Chiang, Y.M. Towards High Power High Energy Aqueous Sodium-Ion Batteries: The  $\text{NaTi}_2(\text{PO}_4)_3/\text{Na}_{0.44}\text{MnO}_2$  System. *Adv. Energy Mater.* **2013**, *3*, 290–294. [[CrossRef](#)]
10. Ma, G.; Zhao, Y.; Huang, K.; Ju, Z.; Liu, C.; Hou, Y.; Xing, Z. Effects of the Starting Materials of  $\text{Na}_{0.44}\text{MnO}_2$  Cathode Materials on Their Electrochemical Properties for Na-Ion Batteries. *Electrochim. Acta* **2016**, *222*, 36–43. [[CrossRef](#)]
11. Kim, H.; Kim, D.J.; Seo, D.H.; Yeom, M.S.; Kang, K.; Kim, D.K.; Jung, Y. Ab Initio Study of the Sodium Intercalation and Intermediate Phases in  $\text{Na}_{0.44}\text{MnO}_2$  for Sodium-Ion Battery. *Chem. Mater.* **2012**, *24*, 1205–1211. [[CrossRef](#)]
12. Zhou, X.; Guduru, R.K.; Mohanty, P. Synthesis and Characterization of  $\text{Na}_{0.44}\text{MnO}_2$  from Solution Precursors. *J. Mater. Chem. A* **2013**, *1*, 2757–2761. [[CrossRef](#)]
13. Sauvage, F.; Laffont, L.; Tarascon, J.M.; Baudrin, E. Study of the Insertion/deinsertion Mechanism of Sodium into  $\text{Na}_{0.44}\text{MnO}_2$ . *Inorg. Chem.* **2007**, *46*, 3289–3294. [[CrossRef](#)] [[PubMed](#)]
14. Zhao, L.; Ni, J.; Wang, H.; Gao, L.  $\text{Na}_{0.44}\text{MnO}_2$ -CNT Electrodes for Non-Aqueous Sodium Batteries. *RSC Adv.* **2013**, *3*, 6650–6655. [[CrossRef](#)]
15. Wang, C.H.; Yeh, Y.W.; Wongittharom, N.; Wang, Y.C.; Tseng, C.J.; Lee, S.W.; Chang, W.S.; Chang, J.K. Rechargeable Na/ $\text{Na}_{0.44}\text{MnO}_2$  Cells with Ionic Liquid Electrolytes Containing Various Sodium Solutes. *J. Power Sources* **2015**, *274*, 1016–1023. [[CrossRef](#)]
16. Xu, M.; Niu, Y.; Chen, C.; Song, J.; Bao, S.; Li, C.M. Synthesis and Application of Ultra-Long  $\text{Na}_{0.44}\text{MnO}_2$  Submicron Slabs as a Cathode Material for Na-Ion Batteries. *RSC Adv.* **2014**, *4*, 38140–38143. [[CrossRef](#)]
17. Kim, D.J.; Ponraj, R.; Kannan, A.G.; Lee, H.W.; Fathi, R.; Ruffo, R.; Mari, C.M.; Kim, D.K. Diffusion Behavior of Sodium Ions in  $\text{Na}_{0.44}\text{MnO}_2$  in Aqueous and Non-Aqueous Electrolytes. *J. Power Sources* **2013**, *244*, 758–763. [[CrossRef](#)]
18. Ruffo, R.; Fathi, R.; Kim, D.J.; Jung, Y.H.; Mari, C.M.; Kim, D.K. Impedance Analysis of  $\text{Na}_{0.44}\text{MnO}_2$  Positive Electrode for Reversible Sodium Batteries in Organic Electrolyte. *Electrochim. Acta* **2013**, *108*, 575–582. [[CrossRef](#)]
19. Shen, K.Y.; Miklos, L.; Wang, L.; Axelbaum, R.L. Spray Pyrolysis and Electrochemical Performance of  $\text{Na}_{0.44}\text{MnO}_2$  for Sodium-Ion Battery Cathodes. *MRS Commun.* **2017**, *7*, 74–77. [[CrossRef](#)]
20. Qiao, R.; Dai, K.; Mao, J.; Weng, T.C.; Sokaras, D.; Nordlund, D.; Song, X.; Battaglia, V.S.; Hussain, Z.; Liu, G.; et al. Revealing and Suppressing Surface Mn(II) Formation of  $\text{Na}_{0.44}\text{MnO}_2$  Electrodes for Na-Ion Batteries. *Nano Energy* **2015**, *16*, 186–195. [[CrossRef](#)]
21. Dai, K.; Mao, J.; Song, X.; Battaglia, V.; Liu, G.  $\text{Na}_{0.44}\text{MnO}_2$  with Very Fast Sodium Diffusion and Stable Cycling Synthesized via Polyvinylpyrrolidone-Combustion Method. *J. Power Sources* **2015**, *285*, 161–168. [[CrossRef](#)]
22. Zhan, P.; Wang, S.; Yuan, Y.; Jiao, K.; Jiao, S. Facile Synthesis of Nanorod-like Single Crystalline  $\text{Na}_{0.44}\text{MnO}_2$  for High Performance Sodium-Ion Batteries. *J. Electrochem. Soc.* **2015**, *162*, A1028–A1032. [[CrossRef](#)]
23. Liu, Q.; Hu, Z.; Chen, M.; Gu, Q.; Dou, Y.; Sun, Z.; Chou, S.; Dou, S.X. Multiangular Rod-Shaped  $\text{Na}_{0.44}\text{MnO}_2$  as Cathode Materials with High Rate and Long Life for Sodium-Ion Batteries. *ACS Appl. Mater. Interfaces* **2017**, *9*, 3644–3652. [[CrossRef](#)] [[PubMed](#)]
24. Hosono, E.; Matsuda, H.; Honma, I.; Fujihara, S.; Ichihara, M.; Zhou, H. Synthesis of Single Crystalline Electro-Conductive  $\text{Na}_{0.44}\text{MnO}_2$  Nanowires with High Aspect Ratio for the Fast Charge-Discharge Li Ion Battery. *J. Power Sources* **2008**, *182*, 349–352. [[CrossRef](#)]
25. Hosono, E.; Saito, T.; Hoshino, J.; Okubo, M.; Saito, Y.; Nishio-Hamane, D.; Kudo, T.; Zhou, H. High Power Na-Ion Rechargeable Battery with Single-Crystalline  $\text{Na}_{0.44}\text{MnO}_2$  Nanowire Electrode. *J. Power Sources* **2012**, *217*, 43–46. [[CrossRef](#)]
26. Li, F.; Ran, J.; Jaroniec, M.; Qiao, S.Z. Solution combustion synthesis of metal oxide nanomaterials for energy storage and conversion. *Nanoscale* **2015**, *7*, 17590–17610. [[CrossRef](#)] [[PubMed](#)]

27. Aruna, S.T.; Mukasyan, A.S. Combustion synthesis and nanomaterials. *Curr. Opin. Solid State Mater. Sci.* **2008**, *12*, 44–50. [[CrossRef](#)]
28. Mumme, W. The Structure of  $\text{Na}_4\text{Mn}_4\text{Ti}_5\text{O}_{18}$ . *Acta Crystallogr. Sect. B Struct. Sci. Cryst. Eng. Mater.* **1968**, *24*, 1114–1120. [[CrossRef](#)]
29. Dall'Asta, V.; Buchholz, D.; Chagas, L.G.; Dou, X.; Ferrara, C.; Quartarone, E.; Tealdi, C.; Passerini, S. Aqueous Processing of  $\text{Na}_{0.44}\text{MnO}_2$  Cathode Material for the Development of Greener Na-Ion Batteries. *ACS Appl. Mater. Interfaces* **2017**, *9*, 34891–34899. [[CrossRef](#)] [[PubMed](#)]
30. Qiao, L.; Swihart, M.T. Solution-phase synthesis of transition metal oxide nanocrystals: Morphologies, formulae, and mechanisms. *Adv. Coll. Interface Sci.* **2017**, *244*, 199–266. [[CrossRef](#)] [[PubMed](#)]
31. Fu, B.; Zhou, X.; Wang, Y. High-Rate Performance Electrospun  $\text{Na}_{0.44}\text{MnO}_2$  Nanofibers as Cathode Material for Sodium-Ion Batteries. *J. Power Sources* **2016**, *310*, 102–108. [[CrossRef](#)]
32. He, X.; Wang, J.; Qiu, B.; Paillard, E.; Ma, C.; Cao, X.; Liu, H.; Stan, M.C.; Liu, H.; Gallash, T.; et al. Durable High-Rate Capability  $\text{Na}_{0.44}\text{MnO}_2$  Cathode Material for Sodium-Ion Batteries. *Nano Energy* **2016**, *27*, 602–610. [[CrossRef](#)]



© 2018 by the authors. Licensee MDPI, Basel, Switzerland. This article is an open access article distributed under the terms and conditions of the Creative Commons Attribution (CC BY) license (<http://creativecommons.org/licenses/by/4.0/>).